Characterizing Flood Impact on Swiss Floodplains Using Interannual Time Series of Satellite Imagery

Gillian Milani, Mathias Kneubühler, Diego Tonolla, Michael Doering, and Michael E. Schaepman

***Abstract*—Pressure on the biodiversity of ecosystems along many rivers is growing continuously due to the increasing number of hydropower facilities regulating downstream flow and sediment regimes. Despite a thorough understanding of the short-term processes and interactions at this hydro-biosphere interface, long-term analyses of the impacts on floodplain dynamics are lacking. We used interannual Landsat 4, 5, 7, and 8 time series to analyze the effects of hydrological events on floodplain vegetation in four mountainous floodplains in the Swiss Alps. Using a spectral mixture analysis approach, we demonstrate that the floodplain vegetation dynamics of mountainous rivers can be recovered at a spatial resolution of 30 m. Our results suggest that interactions between floods and floodplain vegetation are complex and not exclusively related to flood magnitude. Of the four reaches analyzed, only data gathered along the submountainous reach with a quasi-natural flow regime show a clear link between remotely sensed vegetation indices and floods. In addition, our 29-year time series shows a continuous upward trend in vegetation indices along the floodplains, strongest in the reaches affected by hydropower facilities. The approach presented in this study can be easily replicated in other mountain ranges by providing available flow data to verify the impact of hydropower on floodplain vegetation dynamics.**

***Index Terms*—Alps, floods, landsat, normalized difference vegetation index (NDVI) dynamics, unmixing.**

I. Introduction

RIVERS and their floodplains provide essential ecosystem services worldwide while under pressure from hydropower production, agricultural expansion, and climate change [1]–[3]. The changes imposed on the flow regime largely impact the floodplain vegetation through the modification of natural hydrogeomorphic processes [4], since the forms of floodplain vegetation are largely related to flood and sediment characteristics [5], [6]. Alterations of the flow regime, as well as alterations of the sediment transport, result in changes in the floodplain ecosystem, such as vegetation encroachment or increase in nonwoody vegetative cover, but prediction of changes are challenging [7], [8]. Observation and monitoring of floodplain vegetation development and recovery are crucial to assess flow regime management needs and the achievements of restoration projects along river systems globally [9].

A. Floodplain Vegetation Dynamics

The processes linking vegetation to the flow regime have already been the subject of several studies showing strong correlations between flow disturbance and vegetation growth [10]–[12]. Effects of the water flow on the alluvial vegetation can be summarized in six main factors [13], which are, in brief, erosion, asphyxiation of roots, change in floodplain morphology, variations in ground-water, seed dispersal, and change in soil chemistry. Flood events with their timing duration, frequency and magnitude are major components of the flow regime affecting these factors and overall floodplain vegetation [14], [15]. Although changes in floodplain characteristics have been linked to flooding, vegetation development appears to have a more complex relationship with the flow regime [16]. Thus, water flow sustaining an integrity of downstream ecosystems depends on their dynamic character [17], [18]. Considering the complex impact of flow regimes and floods including their magnitude, timing, and duration on alluvial vegetation, the analysis of time series spanning consecutive years could help at understanding these impacts. Such understanding can be helpful for managing flow regimes and reducing the impact of flow alteration on floodplain ecosystems.

In this frame, temporal series of remotely sensed data allow to study vegetation changes and vegetation health status linked to flood events, as well as vegetation recovery. A study by Bertoldi *et al.* [19] demonstrated the usefulness of medium spatial resolution satellite imagery over the Tagliamento river in Italy, where changes in riparian vegetation caused by changes in natural flow conditions were successfully observed.

B. Remote Sensing of Mountainous and Submountainous Floodplains

Despite decades of research on the use of satellite remote sensing for floodplain vegetation [20], its actual use for mountainous and submountainous floodplain studies is still very rare. The study of mountainous and submountainous floodplains based on archive data is challenging because of the relatively small size of the study object compared to the imagery spatial resolution. High or medium-resolution satellite images were used to delimit geomorphological units, flood extent, and land use in riverine

Manuscript received October 30, 2019; revised January 16, 2020 and February 20, 2020; accepted March 7, 2020. Date of publication April 2, 2020; date of current version April 23, 2020. This research project was part of the National Research Programme "Energy Turnaround" (NRP 70, www.nrp70.ch) of the Swiss National Science Foundation (SNSF, Project No. 153972). *(Corresponding author: Gillian Milani.)*

Gillian Milani, Mathias Kneubühler, and Michael E. Schaepman are with the University of Zürich CH-8057, Zürich, Switzerland (e-mail: gillian.milani@geo.uzh.ch; mathias.kneubuehler@geo.uzh.ch; michael.schaepman@geo.uzh.ch).

Diego Tonolla and Michael Doering are with the Institute of Natural Resource Sciences, Zürich University of Applied Sciences CH-8820, Wädenswil, Switzerland, and also with the eQcharta GmbH Tiefenhofstrasse 68 CH-8820, Wädenswil, Switzerland (e-mail: tono@zhaw.ch; doei@zhaw.ch).

Digital Object Identifier 10.1109/JSTARS.2020.2980381

environment, for example by using the ASTER sensor [19] or the QuickBird Satellite sensor [21]. High-resolution satellite imagery has also been used to map bar crest movement over a relatively short time scale [22] or to map riparian habitat at high spatial resolution [23]. Although high-resolution imagery can be useful for studying mountainous and submountainous floodplains [24], [25], the lack of large data archives of high-resolution images hinders their use for interannual studies. Furthermore, coarse resolution imagery, e.g., from the MODIS sensor [26], offering long time series are not suitable in the riverine context given the relatively small size of mountainous and submountainous floodplains.

Among the data archives available today, the Landsat archive offers a unique homogeneous dataset available since several decades and usable at a decameter scale [27], [28]. Landsat Tasseled Cap interannual products have been used to classify the land cover of large floodplains and interannual changes [29], [30]. In the past, previous studies have shown that decameter scale satellite imagery can be used for studying floodplains in a multitemporal setting [19], [31], [32]. However, these studies did not consider a statistical regression analysis with auxiliary datasets such as discharge data and, where limited in the automation of the information extraction from the image stack, limiting, therefore, the number of scenes considered.

In our study, we contribute to the discussion on riparian vegetation changes led by modification of flow regime in mountainous and submountainous rivers by developing a workflow to extract vegetation indices distributions in a semiautomated manner from a data archive suitable to be used for floodplain monitoring, which allows us to carry out a statistical analysis with discharge data from gauging stations. We apply this approach to time series of images geo-located over four Swiss Alpine river floodplains. Our approach allows extracting information on vegetation dynamics covering a very restricted area of the remotely sensed data thanks to spectral mixture analysis (SMA) and an iterative construction of a floodplain mask. The analysis of satellite imagery in our study provides information on the state of riparian vegetation, such as the rate of vegetation growth to be linked to changes in the flow regime. Typical impacts of flow alteration include stream narrowing, vegetation encroachment, and bank stabilization [33], [34]. Compared to natural floodplains showing a correlation between flow regimes including flood events and vegetation dynamics, we expect a decoupling of such mutual effects along floodplains with altered flow and sediment regimes. This hypothesis is motivated by the loss in habitat dynamics expected along reaches with an altered flow regime in particular with lacking flood events. We assume that observed changes in vegetation conditions are mainly triggered by flood events affecting the floodplains.

II. Material and Methods

A. Study Sites

The four Swiss Alpine study sites were selected on reaches of the Sense, Allenbach, Maggia, and Brenno river floodplains where unvegetated gravel bars are large enough to be detected by the remote sensing data considered (see Fig. 1). We selected the four reaches in a way that different states of water flow alteration

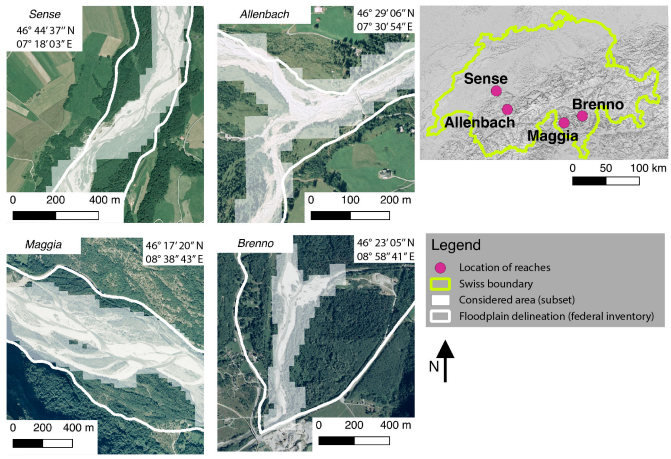

Fig. 1. Subsets of the considered reaches exhibiting the delineation of the floodplains (white line) and the total considered area in the study (white pixels). The floodplain delineations are extracted from the Swiss federal inventory of floodplains of national importance. The total considered area (in white) represents all locations that were included in the mask for the normalized difference vegetation index (NDVI) and the vegetation fraction (VF) calculation for at least one acquisition in the time series. The coordinates refer to the image center. Background Image Source: Orthophotos of the years 2004 and 2005 (Swissimage Geodata © Swisstopo).

can be compared with reaches largely influenced by water flow alterations and others as close as possible to a natural state, under the limits of data availability. The width of the floodplains considered is, therefore, linked to the theoretical minimum width required for a continuous detection of the surface, which encompasses two pixels. This minimum width is here 60 m on the ground, given that the imagery used has a 30 m spatial resolution. The study area was delineated by the extent of the Swiss federal inventory of floodplains of national importance. The last inventory was carried out from 2012 to 2017. The selected reaches each have a gauging station few kilometers upstream or downstream of the reaches of interest. A summary of some of the characteristics of each reach is presented in Table I.

The first reach is located along the Sense river next to the village of Plaffeien, an investigation site of previous studies about its hydromorphology [35], floodplain habitats [36], and the use of aerial imagery [37]–[39]. The Sense river is one of the last rivers in Switzerland to have a near natural flow and sediment regime.

The second reach is located along the Allenbach, a mountainous stream located next to the village of Adelboden. The Allenbach is prone to flood events triggered by short storm events due to the low storage capacity of the watershed [40]. Supplementary information on the Allenbach watershed can be found in [41].

The third reach is located along the Maggia river, between the villages of Boschetto and Lodano. A large hydropower system, Officine Idroelettriche della Maggia SA, impacts the floodplain ecosystem due to flow regulation since circa 1995, resulting in a residual flow regime [42]. The flow regulation has led to a 75% decrease in the average annual discharge, while the annual peak discharge was not decreased [42]. Supplementary information on the flow and sediment dynamics can be found in [43] and, along with landscape composition information in [36].

TABLE I
CHARACTERIZATION OF THE STUDY REACHES IN THEIR ACTUAL STATE

	Maggia	Brenno	Sense	Allenbach
Strahler number	7	6	6	4
Lengh [km]	8	4	4	2.2
Mean floodplain width [m]	304	104	163	128
Area [ha]	243	42	65	28
Mean Elevation [m asl]	365	447	820	1'470
Natural Hydrological Regime	meridional nivo-pluvial	meridional nivo-pluvial	transition nival	meridional nivo-pluvial
Distance to GS [km]	3.5, upstream	1, downstream	15, downstream	0, downstream
Distance to upstream HP [km]	5.3	8	-	-
Substrata	C (hills) / U (valley)	C and S (hills) / U (valley)	U	U / S

The natural flow regime was extracted from data made available by the Swiss Federal Office for the Environment (FOEN). The substrata classification is based on the map GK500 of the Swiss Geotechnical Commission. The width refers to the mean of the detected floodplain area based on the satellite imagery. Abbreviations: GS: gauging station, HP: hydropower plant, C: crystalline, U: unconsolidated, S: sedimentary.

The fourth reach is located along the Brenno river. The reach considered along the Brenno spans a total length of circa 4 km, which we divided into three sections. Such division was necessary to eliminate river sections along which agriculture and roads were close to the channel and, thus, would influence the retrieval of the vegetation indices. The first section is located next to the village of Loderio, the second is located upstream of the village of Motto Blenio, and the third section is located next to the village of Prugiasco. This reach has also been affected by hydropower facilities since circa 1960, leading to a 73% decrease of annual discharge and a substantial decrease in small and medium-sized floods, while the number of flood events does not show any change [44].

B. Satellite Imagery

Our methodology was developed to reflect changes in vegetation indices in medium-resolution satellite imagery (ground resolution ∼30 m), with the aim of using time series covering three decades along mountainous and submountainous rivers. Here, the size of the objects under study was considered to be small for a remote sensing application since the extent of the minimum size under consideration (i.e., the minimal width of the floodplains) is of the same magnitude as the size of the ground sampling distance of the imagery.

Since vegetation indices tend to accurately capture differences in vegetation cover at low fractional cover [45], we make use of the large variation in fractional cover typically found in mountainous floodplains for a robust retrieval of vegetation properties by remote sensing. The central idea is, therefore, to focus on the sparse vegetation areas of the floodplain in order to extract reliable information on changes in vegetation conditions.

We used remotely sensed images acquired by Landsat missions 4, 5, 7, and 8 to construct an interannual time series of vegetation indices [46]. Independent time series were built for each reach. A list of all selected images can be found in the additional material (see Appendix A). The calibrated top-of-atmosphere reflectance [47] at a resolution of 30 m was used. For each reach, only one image was selected per year from 1988 to 2016. This period was chosen as a compromise between data availability, the size of the dataset and the occurrence of large-scale flood events in the sectors of interest. The best image was selected based on minimum cloud coverage over the target area and an acquisition date as close as possible to July 31 to represent the vegetation period. The images used were all from the Landsat series, including the operational land imager (OLI) on Landsat 8, the enhanced thematic mapping system Plus (ETM+) on Landsat 7 and the thematic mapping instrument on Landsat 5 (TM05) and Landsat 4 (TM04). Limiting our analysis to the Landsat image collection allowed a consistent comparison of the information remotely acquired over the period. Where possible, we tended to include data from a single sensor in order to further minimize the biases that could occur due to small but existing differences in sensor characteristics [48]. Therefore, when available, Landsat 7 was chosen instead of Landsat 5, and Landsat 5 images instead of Landsat 4 images. If no suitable images were found in July or August, the images acquired in June were considered as potential candidates. The images from ETM+ were chosen to minimize the scan line corrector (SLC) problem [49]. If the SLC issue affected a large part of the area of interest, images of OLI and TM05 were considered instead.

Although we did not apply atmospheric correction ourselves, we provide some details on these corrections here since the results of this study depend on these processing steps. We used already atmospherically corrected images, as provided by the USGS via the Google Earth Engine platform. The image acquisitions by TM04, TM05, and ETM+ have been corrected using the LEDAPS algorithm (Landsat Ecosystem Disturbance Adaptive Processing System) [50]. Average residues of ∼0.004 to 0.010 have been reported for the accurate recovery of the surface reflectance of ETM+ [51]. Image acquisitions by OLI were corrected using the Landsat Surface Reflectance Code (LaSRC). While LEDAPS uses meteorological services to evaluate the parameters of atmospheric correction, LaSRC uses parameters estimated from the MODIS satellite constellation. The surface reflectance is considered to be captured more accurately by OLI than by previous sensors [52], [53]. We selected only images without clouds or shadows on or close to the reaches. On

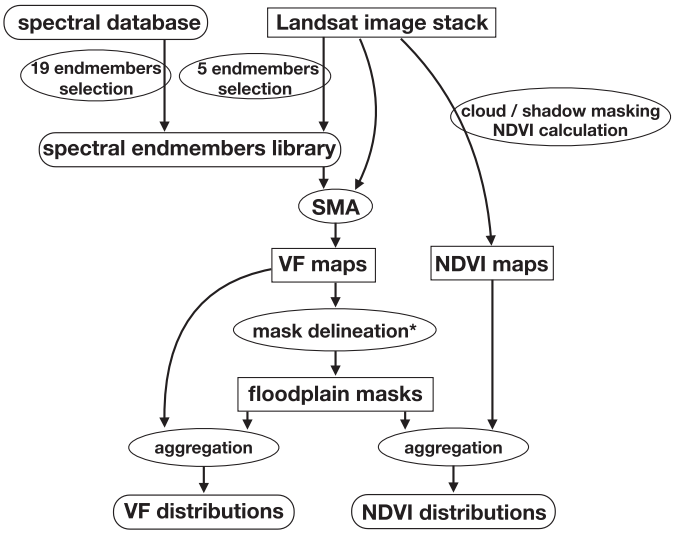

Fig. 2. Schematic workflow from the image stack and spectral endmembers library to the distribution of NDVI and VF. Image or map data are shown as rectangle, nonimage data are shown as rounded rectangle, and operations are shown as the ellipse. The iterative steps of the mask delineation (*) are detailed in Fig. 3.

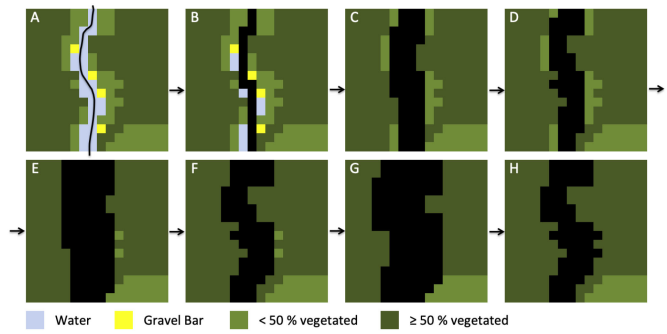

Fig. 3. Scheme of the mask delineation. The center line is first manually (a) digitized and then (b) rasterized. Then, iterations of mask (c), (e), (g) expansion and (d), (f), (h) filtering are applied up to a maximum of six iterations (here three iterations in the scheme). The very last step of mask expansion is not shown here.

each image, the cloud and shadow areas were masked according to the internal flags available in the product quality assessment layer.

C. Image Postprocessing and Vegetation Indices

The normalized difference vegetation index (NDVI) [54] was used in our study, along with fractional vegetation extracted from SMA [55]. The extraction of information from remotely sensed data is realized in multiple steps (see Fig. 2), detailed further as: the building of a spectal endmember library, the production of indices maps, the delineation of the floodplain, and the data aggregation at the reach level.

NDVI varies according to the leaf area index and vegetation health among other sources of variation [56], [57]. NDVI has been used in a broad range of applications such as estimation of productivity, response to environmental changes or trophic interactions [58]. However, NDVI has shown some inconsistencies in a few cases when comparing the state of vegetation at a given location over time [59], [60], e.g., when comparing images acquired under different atmospheric conditions or with different sensors.

To complement the use of NDVI, we also extracted the vegetation fraction (VF) for each pixel, derived from SMA. SMA, or unmixing, aims at retrieving the abundances of a number of selected spectra from a single pixel. A spectral library can be formed from the selected spectra, called spectral endmembers (i.e., a spectral library consists of spectra of different land cover types). The SMA uses a restricted selection of endmembers to estimate the contribution of land cover components to the measured reflectance. For each pixel, the output of the SMA is, therefore, an estimation of covered fraction by each component. In short, SMA retrieves the contribution of each material by an optimal mixture of selected endmembers that create the observed reflectance. The sparse vegetation and small patches of vegetation found on floodplains underpin the need for SMA (see Fig. 1). While it has been shown that nonlinearity is important to retrieve accurate subpixel fractions [61], [62], we are here interested in relative changes, making the retrieval of absolute values not a necessity. For this reason, we consider the VF as an index in our study. Here, we used an implementation of a fully constrained linear spectral unmixing algorithm provided by the Google Earth Engine platform. We used a selection of 19 spectra from the ASTER spectral library as spectral endmembers [63]. Among the 19 selected endmembers, three were vegetation spectra. To complement the selected 19 endmembers, we included three additional vegetation endmembers and two rock material endmembers extracted specifically from the selected images, leading to a total of 24 endmembers.

The image postprocessing creates three products, i.e., 1) the delineation of a floodplain mask (see Fig. 3), 2) the extraction of the NDVI distribution, and 3) the extraction of the VF distribution. The mask was created from the same center line for each year. First, we digitized a line in the center of the unvegetated area. The line was then rasterized, defining an initial mask at a resolution of 30 m. Then, two steps were repeated iteratively. First, the initial mask was extended by one pixel in all directions. Then, pixels that contain a VF larger than or equal to 50% were removed from the mask. The threshold of 50% was based on a qualitative consideration of the non-forested areas inside the retrieved mask compared to the federal inventory of floodplains (updated on July 1, 2007) issued by the Swiss Federal Office for the Environment (FOEN). Repeating these steps several times results in a mask that covers all pixels in the section that have a VF smaller than 50 percent. Six repetitions extend the mask to a maximum width of 360 m. The last step in the construction of the mask consisted of a final expansion of one pixel in all directions. This last step creates a mask robust to one-pixel variations of coregistration. The distributions of the NDVI and VF values were finally extracted for each year within the limits defined by the mask.

The theoretical range of NDVI is from -1 to 1. Negative values can be found over water bodies. The low positive values observed here generally correspond to bare soils, areas of unvegetated gravel, or a mixture of gravel and water. In general, the

TABLE II
COEFFICIENT OF SPEARMAN'S RANK CORRELATION FOR THE MASK SIZE (MS), NDVI, AND VF CHANGES AGAINST THE FLOW VARIABLES FOR THE FOUR REACHES

	Sense			Allenbach			Maggia			Brenno		
	MS	NDVI	VF	MS	NDVI	VF	MS	NDVI	VF	MS	NDVI	VF
Q2	-	-0.52	-0.65	-	-	-	-	-	-	-	-	-
Q10	-	-0.5	-0.64	-	-	-	-	-	-	-	-	-
Q30	-	-	-	-	-	-	-	-	-	-	-	-
Qmax	-	-0.55	-0.65	-	-	-	-	-	-	-	-	-
NM7Q2	-	-	-	-	-	-	0.54	-	-	-	-	-
Q2 spring	-	-	-0.52	-	-	-	-	-	-	-	-	-
Qmax spring	-	-0.4	-0.53	-	-	-	-	-	-	-	-	-
NM7Q2 spring	-	-	-	-	-	-	0.43	-	-	-	-	-

Only the correlation coefficients statistically significant at an alpha value of 0.05 are shown.

NDVI increases with vegetation cover and vegetation health. The possible values of VF range from 0 to 1. A VF value of 0 indicates a total absence of vegetation within a pixel, while a VF value of 1 indicates that the entire pixel is covered with vegetation. An intermediate value indicates that parts of the pixel are covered with vegetation. An intermediate value can be observed over different configurations, for example, if vegetation is sparse or because there is a clear boundary between land cover types. Also, intermediate values of NDVI and VF may indicate the presence of large woody debris in the pixel. It is indeed almost impossible to differentiate between very sparse vegetation and the presence of woody debris in a pixel because of the similar spectral signature of the two types of land cover.

D. Flow Variables

The discharge data were made available by the Swiss Hydrology Division of the FOEN.

We chose gauging stations as close as possible to the study reaches (see Fig. 1): Maggia - Bignasco, Ponte Nuovo 2475, Brenno - Loderio 2086, Allenbach - Adelboden 2232, and SenseThörishaus, Sensematt 2179.

Eight variables, which are expected to be related to floodplain vegetation dynamics, were calculated from maximum daily flow data of the selected hydrological stations for each period between satellite images (see Table VII). Only flow data until the exact image acquisition date were considered as part of the period. For example, if a satellite image was acquired over the Sense on July 17, 2014, the flood occurring on August 11, 2014, was then considered in the subsequent period (image 2015). The eight flow variables used in the analysis were as follows.

1) *Q2*, *Q10*, and *Q30:* number of floods with return periods of n = 2, 10, and 30 years. Commonly used to describe recurrence of floods with a certain magnitude [64]. *Qn* were extracted from the FOEN report for each gauging station, without catchment correction. For example, a *Q2* event is defined here as a day presenting a peak discharge equal or higher than the *Q2* discharge. A flood can be considered in multiple groups (i.e., if one *Q10* occurred, it was also considered as *Q2*, since it raises above both thresholds).
2) *Qmax:* yearly maximum discharge [65], [66].
3) *NM7Q2:* number of days with a daily average discharge lower than the lowest average discharge observed over seven consecutive days with a return period of two years (extracted from the FOEN reports). Commonly used to describe the effect of droughts periods [67].
4) *Q2 spring*, *Qmax spring*, *NM7Q2 spring: Q2*, *Qmax,* and *NM7Q2* for the same growing season as the image acquisition, defined as starting from the first of April and lasting until the date of the image acquisition.

We, then, calculated the Spearman's rank correlation between the eight flow variables and the changes in NDVI median and VF median. A threshold of significance was set at an alpha value of 0.05 for the correlation. The number of correlations being significant is inflated due to the number of tests carried out. However, we did not apply a correction for balancing the presence of false-positive results due to the limited sample size. Instead, we relied on the coherence between correlations being significant at an alpha value of 0.05 to interpret them together.

III. RESULTS

A. Spearman's Rank Correlation

The *Q2*, *Q10* and *Qmax*, and *Qmax spring* variables were negatively correlated at a significance level of 0.05 with changes in NDVI and VF along the Sense (see Table II). Correlation coefficients were slightly higher for VF changes than for NDVI. Variables limited to the spring period showed similar statistical trends as the full-year variables, although they have lower correlation coefficients. Along the Maggia, the variables *NM7Q2* and *NM7Q2 spring* showed a statistically significant relationship with the change in mask size. No significant relationship was found between flow variables and variation of indices along the Allenbach and Brenno rivers.

Along the Sense, the regression between the occurrence of *Q2* events and the change in NDVI was examined more closely (see Fig. 4). The more detailed logistic model was restricted to the Sense, since the other reaches did not show statistical relations between the median of the indices and the flow variables. In particular, along the Sense, about half of the years in which at least one *Q2* event was present showed a negative change in the indices larger than the most extreme change observed without

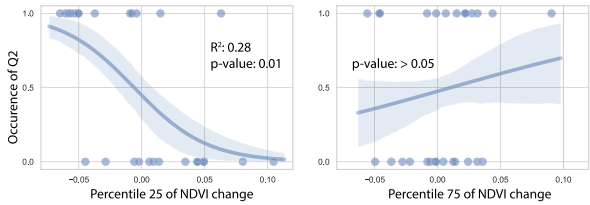

Fig. 4. Logistic regression between the NDVI and the occurrence of preceding *Q2* events. For each image acquisition, absence of preceding events leads to a value of 0 and presence of at least one preceding *Q2* event leads to a value of 1.

preceding *Q2* events. A logistic model was, therefore, tested between the occurrence of *Q2* events and percentiles of NDVI distribution. On the one hand, the 25th percentile of the NDVI distribution was correlated at a significance level of 0.05 with the occurrence of at least one *Q2* event. However, 75th percentile of the NDVI distribution was not significantly correlated with the occurrence of *Q2* events. A very similar result was obtained from the VF distributions (see Fig. 5).

B. Indices Dynamics

Besides statistical analysis, a qualitative analysis between individual events and changes in indices was carried out (see Fig. 6).

In general, along the Sense, the Maggia, and the Brenno rivers, presence of *Q10* or *Q30* events coincides with a decrease in indices. Periods with few flood events exhibit an increase in indices, such as from 1990 to 2005 along the Sense, from 2002 to 2007 along the Maggia (particularly on the NDVI), and from 1994 to 1999 and 2009 to 2015 along the Brenno. Along the Sense, the large flood event of 1990 (489 m^3/s, return period: $>$150 years) coincided with an observed decrease in NDVI and VF, although the magnitude of the decrease is not as unique in the time series as the peak discharge.

Along the Allenbach, no pattern is qualitatively visible in the dynamics of the indices. The low VF values found in 2014 and 2015 coincided with relatively dry periods preceding the image acquisitions. Also along the Allenbach, the second part of the time series, from 2003 to 2016, showed some positive statistical relation between changes in indices and the occurrence of large floods, although this was not significant (see Figs. 7 and 8).

Overall, the NDVI values showed less variability than the VF values, both for mean values and for complete distributions (violin charts, Appendix D). The presence of a statistical mode in the upper half of the NDVI and VF distributions, around 0.7 and 0.9, respectively, represents pixels that are found on entirely vegetated areas. Another mode in the lower half of the NDVI and VF distributions, around 0.3 and 0.1, respectively, typically represents pixels that are completely free of vegetation.

C. Trend in the Time Series

The trends of the indices over the years were analyzed. Overall, the NDVI and VF distributions increased over the years (see Fig. 9). The median of the NDVI showed a significant increase over the years for all four reaches. The median of the VF only increased significantly over the years along the Maggia and Brenno reaches. The coefficient of determination (R^2) of the linear regression on the NDVI along the Maggia river was particularly high at 0.75.

An analysis of the autocorrelation function of the detrended time series did not reveal a significant level of autocorrelation beyond a one-year lag along the Sense, Allenbach, and Brenno rivers. A significant level of autocorrelation was detected with a three-year delay for NDVI along the Maggia river. A significant level of autocorrelation with a one-year lag for all reaches has a small but existing impact on the significance of statistical tests performed on linear trends, which increases the rate of Type I error.

IV. Discussion

A. Relation Between Flow Variables and Remote Sensing Indices

1) Sense Reach: Along the Sense river, periods with flood events generally coincide with decreases in NDVI and VF values, while no linear relationships are observed along the other three reaches. The magnitude of the flood events (represented by *Qmax*) and the number of flood events with a return period of 2 and 10 years (*Q2* and *Q10*) are statistically related to changes in the extracted indices. These observations are in line with the general principle that floods are one of the main drivers of habitat dynamics in floodplains [68], [69].

The impact of the major flood of 1990 on the indices (489 m^3/s) is of the same magnitude as for the 2005 and 2014 floods (246 and 299 m^3/s). The 2007 flood had less impact on the indices, probably due to erosion caused by the 2005 flood two years earlier. A remarkable difference between these events can, however, be found in the average daily flow. The average daily flow during the 1990 floods was 34.6 and 32.9 m^3/s on July 29 and 30, respectively, while the average daily flow was 147 m^3/s on July 22, 2005 and 130 m^3s on August 9, 2007. The very short duration of the flood event of 1990 can therefore be part of the explanation of a relatively weak change of indices despite the exceptional character of the flood event. This observation supports the fact that not only the flood peak is important, but also other characteristics such as the duration or the total energy of the flood event [70].

Another fact that can explain the relatively low impact of the flood of 1990 on the indices is that the retrieved indices do not necessarily reflect all the impacts of a flood on the floodplain land cover. Although large floods (*Q50*) have been observed to have significant effects on channel morphology [71], the impacts on floodplain morphology may not be proportionally reflected by the impacts on the riparian vegetation [72].

In addition, the effects of flow regulation on vegetation structure may still be incomplete after several decades [73], which suggest a shaping of floodplains in the long-term rather than single large flood events. These elements can, therefore, explain the lack of change in vegetation indices after a single flood event with a very large peak discharge. Instead, some studies have found a clearer statistical relationship between the frequency of moderate flooding (*Q1* to *Q10*) and changes in vegetation in mountainous and submountainous floodplains [31], [74]. In brief, all this aspects suggest that the lack of prominent impact by

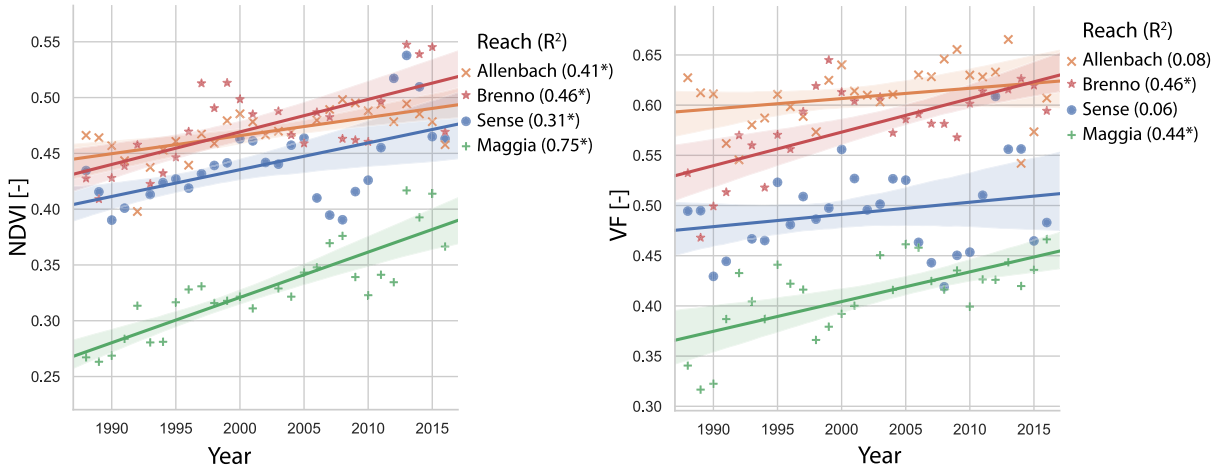

Fig. 5. Logistic regression between the (VF and the occurrence of preceding *Q2* events. Absence of preceding events leads to a value of 0 and presence of at least one *Q2* event leads to a value of 1 for the samples.

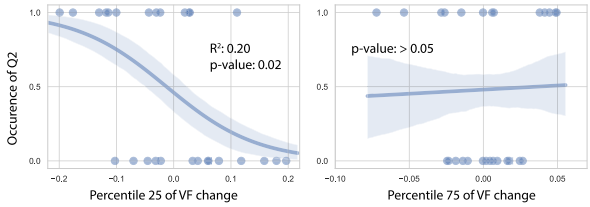

Fig. 6. Mean values of the NVDI and VF from 1988 to 2016 along the four investigated reaches (scale on the left axis) and mask size over which the indices were extracted for each year (right axis). The bands along the curves indicate a 68 percent ($\pm 1\sigma$) confidence interval. The *x*-axis depicts the year of image acquisition. The flood events happening between two acquisitions are centered between the image acquisitions along the *x*-axis. The flood event discs are vertically distributed (close - far) according to the time length preceding the next image acquisition.

the large flood of 1990, although counterintuitive, is in line with a normal common of natural floodplains found in mountainous environment.

2) Maggia and Brenno Reaches: Along the two hydropower affected reaches of the Maggia and Brenno, although we observed a decrease in indices for most major floods, the absence of correlation can be explained by the presence of changes in the indices over years without flood events. The dynamics of the indices along these reaches are presumably related to the alteration of water flow by upstream hydropower facilities, in addition to other factors such as land use change or weather variation. The modification of the natural flow regime by dams or hydropower plants has a strong impact on erosion, transport and sediment deposition [75] along with a variable response of floodplain vegetation [12]. Another study on the Maggia reach indicated that flow changes resulted in a loss of natural vegetation dynamics and a decrease in nonvegetated gravel bars [42]. Since the frequency of large flood events has not decreased [42], the absence of a statistical link between floods and the indices can suggest that the alteration of the sediment regime has a large influence on the development of the vegetation in the floodplains [76].

The co-occurrence of dry periods with an increase in mask size observed along the Maggia is probably related to the canopy leaf angle distribution, which changes the retrieved vegetation-free fraction per pixel in the spectral mixture analysis [77]. Consequently, it is expected that dry periods lead to a higher estimation of the vegetation-free fraction.

Along the Brenno, some years without *Q2* events show a decrease in the indices, leading to an absence of a statistical relationship. The observed decrease in the indices may result, in this case, from a limitation of the chosen approach: the construction of the floodplain mask for each single year may independently mask the areas of the floodplain in which strong plant growth occurs, resulting in a shrinking of the area under consideration and, thus, an "artificial" decrease in the indices. It is not possible to disentangle the effect of the mask size change from other changes without external data. Changes of the mask size are smaller along the other reaches, although present as well.

3) Allenbach Reach: Along the Allenbach, no statistical relation was found between flow variables and indices. In contrast to the Sense, Brenno, and Maggia reaches, the Allenbach floodplain is subject to fast variation in water flow and recurrent flood events due to storms [78]. Given the smaller size of the watershed, the Allenbach is subject to reduced variations in the intensity of flood events compared to the other reaches. This results in a floodplain with almost no presence of pioneer species and a well-defined floodplain boundary. The delimitation between the surrounding vegetation areas and the vegetated zones of the floodplains is clearly defined. Such a floodplain structure is in line with an absence of statistical link between flow variables and NDVI and VF, therefore supporting the method developed in this study, since, as it would be expected along this reach, the flood events have a limited direct impact on the floodplain vegetation.

4) Periods With Few Disturbances: Flood-free years generally coincide with an increase in NDVI and VF (see Fig. 6), although these links are not statistically significant. Vegetation growth in size and space has been observed during periods without flooding [16]. Also, some dynamics in NDVI and VF can be linked to previous floods, most likely representing recovery after a disturbance. Vegetation recovery after a major flood can

occur in the short term [79], [80]. However, the vegetation can still be altered for decades [73]. Periods of increased vegetation productivity following flooding have been observed using coarse resolution imagery in semiarid environments [81]. Although floods are the main source of erosion of floodplain vegetation, they also create conditions favorable to the establishment of seedlings through the deposition of sediment and nutrients [82], [83]. The increase of NDVI and VF distributions after major floods may also be influenced by the deposition of woody debris on sediment bars, islands, and terraces, as it occurs in the Sense river [38], introducing bursts of nutrients to these areas [84], [85]. Finally, the floodplains found in mountainous environment have been described as being very resistant and having a high recolonization capacity [86]. The dynamics observed over flood-free years show the importance of disturbance to support floodplain ecosystems by enabling habitat turnover [31] and, thus supporting establishment of unvegetated gravel bars, as well as pioneer vegetation.

B. Trends in Time Series

The indices retrieved along the Maggia and Brenno reaches and, to a lesser extent, along the Sense and Allenbach reaches, show an increase in the averages of the indices over the period considered. Such an increase in vegetation is in line with observations made in other studies along the Maggia [42] and Brenno [44]. The observed trends in vegetation dynamics may also be related to longer-term climate-related processes [87]. In general, river systems have been described as very sensitive to climate variation [88], [89].

An overall increase in vegetation cover leading to a shrinking of riparian areas is consistent with the expected response to climate change [90], [91]. Changes in the flow regime of the Allenbach and the Sense river can potentially be triggered by climatic variations, since, to our knowledge, no large changes in the land cover have occurred in the watershed for the considered period. For example, from 1950 to 2016, three of the five largest peak discharges recorded by the Sense - Thörishaus station occurred in 2011, 2012, and 2015. A stable increase of the magnitude of *Qmax* is also visible in the flood statistics of the Allenbach - Adelboden station from 2011. Given all these elements, the observed changes in the indices retrieved over the floodplain vegetation may be due to climate variations in the Alps, although they could also be triggered by different causes such as land use changes or a combination of both.

The detected trends in the NDVI values may be partially affected by artifacts present in the satellite imagery. It is also possible, however unlikely given the rigorous calibration of the Landsat time series [49], that a shift in sensor performance affects the NDVI. It has previously been reported that the combination of LC07 acquisitions with TM acquisitions can lead to an artificial underlying trend in NDVI [92]. In addition, some differences were reported regarding the data acquisition by OLI and previous satellites sensors [93]. More specifically, lower values in the visible range were consistently observed for OLI, corresponding to a slight increase in the NDVI. However, the variations of the on-orbit gains (in the order of 0.5%) are lower than our observed dynamics [94]. It is also likely that the VF is less affected by a possible shift in the Landsat series surface reflectance data. In brief, while the NDVI shows a trend along all reaches, suggesting a climate-induced change, the VF index shows a trend only along the Brenno and Maggia rivers, suggesting a change induced by hydropower. In conclusion, while the trends may be affected by sensor performance, they are most likely caused by land use or climatic variations or a combination of them.

C. Sensibility of Remotely Sensed Indices

Four points are discussed in this section as follows:

1) the sensibility of the indices to a real change;
2) the variations in violin charts;
3) the variation in mask size;
4) the influence of the day of year (DOY) of the acquisition.

The VF distribution is known to be sensitive to variations in the spectral characteristics of the land cover [95]. Therefore, changes in the spectral properties of a pixel can lead to variations in the estimated fraction of vegetation. The sensitivity of the VF is visible in the dynamics of the indices: some periods show variations in the VF, while the NDVI remains relatively stable between consecutive years. However, the changes described by SMA may be more accurate than the changes described by NDVI [96], although NDVI and results from SMA are known for providing consistent information over a variety of environments [97].

The violin charts (see Appendix D) revealed that flooding affects the shape of the NDVI and VF distributions by inflating the lower mode. An overall decrease in the two distributions indicates that individual flood events erode parts of the floodplain vegetation. In the representation of the complete distribution (see Appendix D), large variations in VF cannot be entirely attributed to shifts in the presence of vegetation, due to the high temporal resolution of image acquisition relative to the vegetation growth rate at high VF values. Although some pioneer species can develop rapidly on unvegetated gravel bars, some changes in VF associated with high VF values are typical of forest cover. It is, therefore, more likely that the variations observed in the higher mode of VF distribution are related to the reflective properties of the forests and grasslands surrounding the floodplain.

The variability in mask size has an influence on the change of indices. The mask size is expected to be inversely proportional to the average of the indices, since a greening of the floodplain should result in a smaller number of pixels with an FV below the 50% threshold. As a consequence, the NDVI and VF distributions can raise over the years either due to an overall greening or due to a thinning of the floodplain width.

To verify that the trends (see Fig. 9) are not due to a shift of the acquisition time, we calculated the correlation of the DOY of acquisition along the time series. We did not find any coherent bias between early acquisitions and the rest of the time series (only the VF in 2014 along the Allenbach is found to be particularly low among the three earliest samples). We then checked the correlation between DOY of an acquisition and the specific year. The time series along the Maggia reach

consists of decreasing DOY values with increasing years, with a p-value of 0.016 on the null hypothesis stating that the regression slope is zero. Since the trend along Maggia reach is similar to other reaches (see Fig. 9), it is not expected that the DOY of the acquisition influences the results. Finally, given the tree genders found along the reaches composed, among others, of *salix*, *Populus*, *alnus*, the phenology of present plants should not have a large impact on the retrieved NDVI and VF distributions. Most of the tree species along all the considered reaches have a stable phenological state over the period from June to August, inside which the images have been selected.

D. Limitations of Satellite Imagery

The satellite imagery used in our study captures multiple types of land cover changes that occur in a floodplain. However, it is not always possible to clearly separate the various types of change. For example, floods impact vegetation due to erosion from water or floating debris, or by prolonging the saturation of the root zone [98]. Substrate erosion is another cause of vegetation loss that can lead to changes in the indices, however on a longer time scale. The erosion and deposition of substrate influence vegetation growth on the floodplains [99]. Change in resources availability can also lead to changes in the floodplain vegetation. Droughts, for example, have an important influence on floodplain vegetation [100]. Variations in water availability or in nitrogen availability are, however, not easily detectable using satellite imagery. Although water is frequently available for floodplain vegetation, the lack of soil or the relatively coarse size of soil gravel do not store large amounts of water, making floodplain vegetation subject to significant and rapid changes in water availability [101]. Also, the response of riparian vegetation to variation in groundwater can vary [102].

In our observations, the periods of low water discharge are not well retrieved by the remotely sensed indices, although drought events have been observed by remote sensing through the NDVI statistics [103]. The lack of sensitivity can be explained by the fact that the NDVI and VF values recovered in the poorly vegetated areas are mainly related to the proportion of vegetation, rather than the vegetation state. Since a stressful event, such as a drought, primarily affects vegetation health, it is expected that remotely sensed indices will not change substantially, as the relative proportion of vegetation is expected to remain stable. In other words, the variation in NDVI and FV over the floodplains is mainly driven by the vegetation fraction. Another limitation of satellite imagery in our study relates to the description of changes in the sediment dynamics. Since such changes typically involves variation in the floodplain topography, generally without a large impact on the reflectance of the involved land cover, their observations from medium-resolution imagery are very challenging.

As a complementary approach, SAR imagery could be used to generate similar time series of vegetation dynamics along the reaches of interest. Using SAR imagery would allow to validate the obsevations made with an auxiliary data source. While SAR has been used to study floodplain forests [104], [105], it has been less commonly used for observing mountainous and submountains floodplains. In the setting of this study, the capabilities of SAR imagery to map fractional vegetation cover or proxies such as biomass [106] or other vegetation properties [107], [108] would be of interest. However, the use of such an approach in the specific environment of mountainous floodplains would require a careful validation supported by ground measurements.

V. Conclusion

In this section, our observations confirm that satellite time series can support the study of floodplain ecosystems in mountainous and submountainous river floodplains under the influence of flood events. The results suggest that it is important to take into account the sequence of flood events and their magnitude to contextualize the impact of a single flood on floodplain vegetation. To observe vegetation dynamics along rivers, we assessed the state of vegetation using NDVI and VF distributions of remotely sensed vegetation. Using NDVI in combination with a fraction of the vegetation estimated from a spectral mixture analysis has proven to be a robust approach to cloud disturbance and local reflectance variation. Therefore, time series of index distributions can be extracted in a robust way and, thus, be used to study inter-annual dynamics of vegetation conditions.

Overall, flood impacts were visible in the time series of indices averages and in the graphical representation of full indices distributions. The approach chosen in this study is particularly suited to mountainous and submountainous floodplains, which generally have a relatively large area affected by the dynamics of water and sediment flows. We found a statistically significant relationship between changes in NDVI and VF distributions and flooding only along the submountainous reach with a near-natural flow regime. A weak or nonexistent statistical link was found along the altered reaches, as the flow alterations due to hydropower facilities modify or even completely disrupt floodplain dynamics. To perform these analyses, data on water flow, such as discharge measurements, are required. The transfer of the method is, therefore, limited to reaches with adequate sensors and statistics.

In addition, long-term trends in floodplain vegetation development were clearly depicted by the remotely sensed indices. However, it remains unclear whether the observed trends are caused by changes in the flow and sediment regime due to hydropower production, watershed land use, climate variations, partly by sensor performance, or a combination of them. The long-term trends analyses performed are independent from ground data (such as discharge measurement) and are, therefore, easily transferable to any reach where optical satellite imagery is sufficient to describe the land cover.

We believe that the remote sensing approach used in this study can be transferred to other regions of the earth, as it is not based on prior information. Satellite imagery can support river management at the catchment level [109], although the application of this approach appears to be limited to a large extent by the availability of accurate discharge data. Finally, we claim that satellite imagery has great potential, currently untapped, to better understand moutainous and submountainous floodplain dynamics and anthropogenic impact to support the protection of floodplains worldwide.

APPENDIX A
SATELLITE IMAGES

TABLE III
INFORMATION ON SATELLITE TILES USED FOR THE TIME SERIES SENSE 2003–2010

Year	Sensor	Tile	DoY	Discharge
2016	OLI	196027	219	6.17
2015	OLI	196027	184	2.73
2014	OLI	196027	197	6.60
2013	OLI	196027	194	2.34
2012	ETM+	195927	241	2.13
2011	ETM+	195028	222	3.37
2010	ETM+	195027	187	3.96
2009	ETM+	195028	200	8.30
2008	ETM+	195027	230	5.78
2007	ETM+	195027	195	6.57
2006	ETM+	195027	192	4.03
2005	ETM+	196027	228	4.37
2004	ETM+	195027	203	4.12
2003	TM05	196027	215	1.54
2002	ETM+	195028	229	5.50
2001	ETM+	195028	226	3.19
2000	TM05	195028	232	2.85
1999	TM05	195028	197	6.80
1998	TM05	196027	217	2.34
1997	TM05	196027	230	3.26
1996	TM05	195027	221	6.18
1995	TM05	195027	202	4.13
1994	TM05	195027	215	3.23
1993	TM05	196027	187	10.55
1992				
1991	TM05	195028	191	3.77
1990	TM05	195027	220	3.10
1989	TM05	195027	185	6.12
1988	TM04	195028	239	4.73

The *Discharge* column refers to the average daily discharge at the reference station of Sense - Thörishaus, Sensematt 2179. Blank years are due to the absence of appropriate images caused by cloudy conditions. OLI: Landsat 8 Operational Land Imager, ETM+: Landsat 7 Enhanced Thematic Mapper Plus, TM05: Landsat 5 Thematic Mapper, TM04: Landsat 4 Thematic Mapper, DoY: Day of Year.

TABLE IV
INFORMATION ON SATELLITE TILES USED FOR THE MAGGIA REACH

Year	Sensor	Tile	DoY	Discharge
2016	ETM+	195028	188	1.83
2015	OLI	194028	218	1.80
2014	OLI	194028	183	1.87
2013	OLI	195028	203	1.82
2012	ETM+	194028	202	1.85
2011	ETM+	194028	183	1.83
2010	ETM+	194028	212	1.84
2009	ETM+	194028	225	2.00
2008	TM05	195028	206	1.84
2007	TM05	194028	196	1.89
2006	ETM+	194028	201	1.94
2005	TM05	194028	174	1.90
2004	ETM+	194028	180	1.93
2003	TM05	195028	224	1.88
2002				
2001	ETM+	195028	210	2.40
2000	TM05	195028	200	1.96
1999	TM05	194028	206	1.84
1998	TM05	194028	219	1.91
1997	TM05	195028	223	1.95
1996	TM05	194028	214	1.88
1995	TM05	194028	179	2.58
1994	TM05	195028	215	1.92
1993	TM05	195028	228	1.77
1992	TM05	194028	219	1.82
1991	TM05	194028	216	1.84
1990	TM05	194028	229	1.75
1989	TM05	194028	242	1.75
1988	TM05	195028	199	1.76

Please refer to the caption of Table III. The reference station is Maggia - Bignasco, Ponte nuovo 2475.

TABLE V
INFORMATION ON SATELLITE TILES USED FOR THE ALLENBACH REACH

Year	Sensor	Tile	DoY	Discharge
2016	ETM+	195028	220	1.10
2015	OLI	195028	241	0.65
2014	OLI	195028	158	1.42
2013	ETM+	195028	211	1.30
2012	ETM+	195028	193	0.70
2011	ETM+	195028	222	1.10
2010	ETM+	195028	187	1.38
2009	ETM+	195028	200	1.45
2008	ETM+	195028	230	1.29
2007	ETM+	195028	195	2.33
2006	TM05	195028	200	1.21
2005				
2004	TM05	195028	195	0.78
2003	ETM+	195028	216	0.47
2002	ETM+	195028	229	0.92
2001	TM05	195028	202	2.39
2000	ETM+	195028	224	0.91
1999	ETM+	195028	205	0.98
1998	TM05	195028	242	0.39
1997	TM05	195028	207	2.07
1996	TM05	195028	221	0.84
1995	TM05	195028	202	1.21
1994	TM05	195028	215	0.65
1993	TM05	195028	196	1.19
1992	TM05	195028	242	0.59
1991	TM05	195028	175	3.45
1990	TM05	195028	220	0.44
1989	TM05	195028	201	0.78
1988	TM05	195028	231	0.42

Please refer to caption of Table III. The reference station is Allenbach - Adelboden 2232.

TABLE VI
INFORMATION ON SATELLITE TILES USED FOR THE BRENNO REACH

Year	Sensor	Tile	DoY	Discharge
2016	ETM+	194028	197	3.71
2015	OLI	194028	218	1.86
2014	OLI	194028	215	5.43
2013	OLI	194028	212	2.37
2012				
2011	ETM+	194028	183	2.12
2010	ETM+	194028	196	3.05
2009	ETM+	194028	225	3.97
2008	ETM+	194028	239	2.38
2007	TM05	194028	196	3.58
2006	TM05	194028	193	1.43
2005	TM05	194028	174	2.04
2004	ETM+	194028	180	2.46
2003	TM05	194028	217	1.41
2002				
2001	ETM+	194028	203	7.22
2000	ETM+	194028	169	3.24
1999	TM05	194028	206	3.18
1998	TM05	194028	219	2.81
1997	TM05	194028	232	2.91
1996	TM05	194028	230	2.57
1995	TM05	194028	179	3.30
1994	TM05	194028	208	2.77
1993	TM05	194028	157	4.18
1992	TM05	194028	219	2.42
1991	TM05	194028	216	1.72
1990	TM04	194028	189	3.91
1989	TM05	194028	242	2.12
1988	TM05	194028	192	7.76

Please refer to the caption of Table III. The reference station is Brenno - Loderio 2086.

APPENDIX B
COMPLEMENTARY INFORMATION ON THE FLOW VARIABLES

TABLE VII
EXTENDED DEFINITION OF THE FLOW VARIABLES

Q2	Number of days since the last image acquisition with a peak discharge equaling or exceeding the Q2 threshold, being the discharge with a return period of 2 years
Q10	Number of days since the last image acquisition with a peak discharge equaling or exceeding the Q10 threshold, being the discharge with a return period of 10 years
Q30	Number of days since the last image acquisition with a peak discharge equaling or exceeding the Q30 threshold, being the discharge with a return period of 30 years
Qmax	Maximum peak discharge observed since the last image acquisition
NM7Q2	Number of days since the last image acquisition with a peak discharge equaling or below a threshold defined as being the NM7Q with a return period of 2 years (The NM7Q extracted from FOEN report (see manuscript), is defined as "The annual minimum discharge levels recorded during 7 consecutive days").
Q2 spring	Similar to Q2, with flow data restricted from April 1st to the date of image acquisition
Qmax spring	Similar to Qmax with flow data restricted from April 1st to the date of image acquisition
NM7Q2 spring	Similar to NM7Q2 with flow data restricted from April 1st to the date of image acquisition

The thresholds defined for the flow variables (Q2, Q10, Q30, and NM7Q) were extracted from reports made available by the Hydrology Division of the FOEN.

APPENDIX C
COMPLEMENTARY FIGURES ON LINKS BETWEEN FLOOD EVENTS AND INDICES

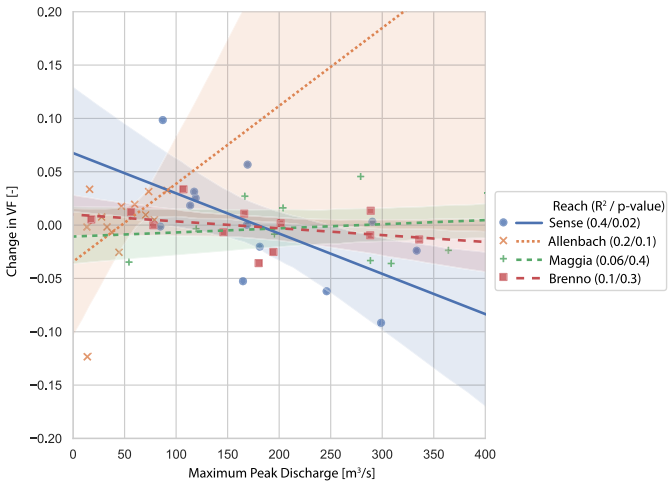

Fig. 7. Linear regression between the maximum peak discharge and the change in the VF along the four reaches for the years 2003 to 2016. A p-value under 0.05 is found for the slope coefficient along the Sense reach.

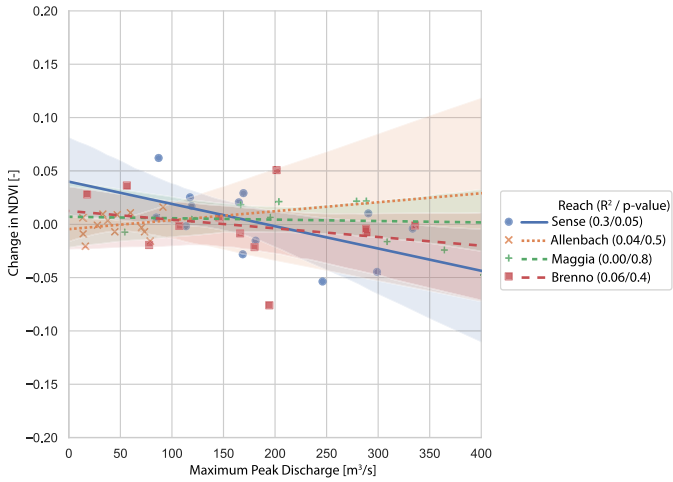

Fig. 8. Linear regression between the maximum peak discharge and the change in the NDVI along the four reaches for the years 2003 to 2016. A p-value if 0.05 is found for the slope coefficient along the Sense reach.

APPENDIX D
COMPLEMENTARY FIGURES OF TIME SERIES

For each time series, we present the distribution of NDVI and VF by violin graphs [110]. The violin graph displays a smoothed kernel density estimation of the underlying histogram. Violin graphs ease the comparison of multiple distributions next to each other by smoothing extreme peaks and reducing the data noise.

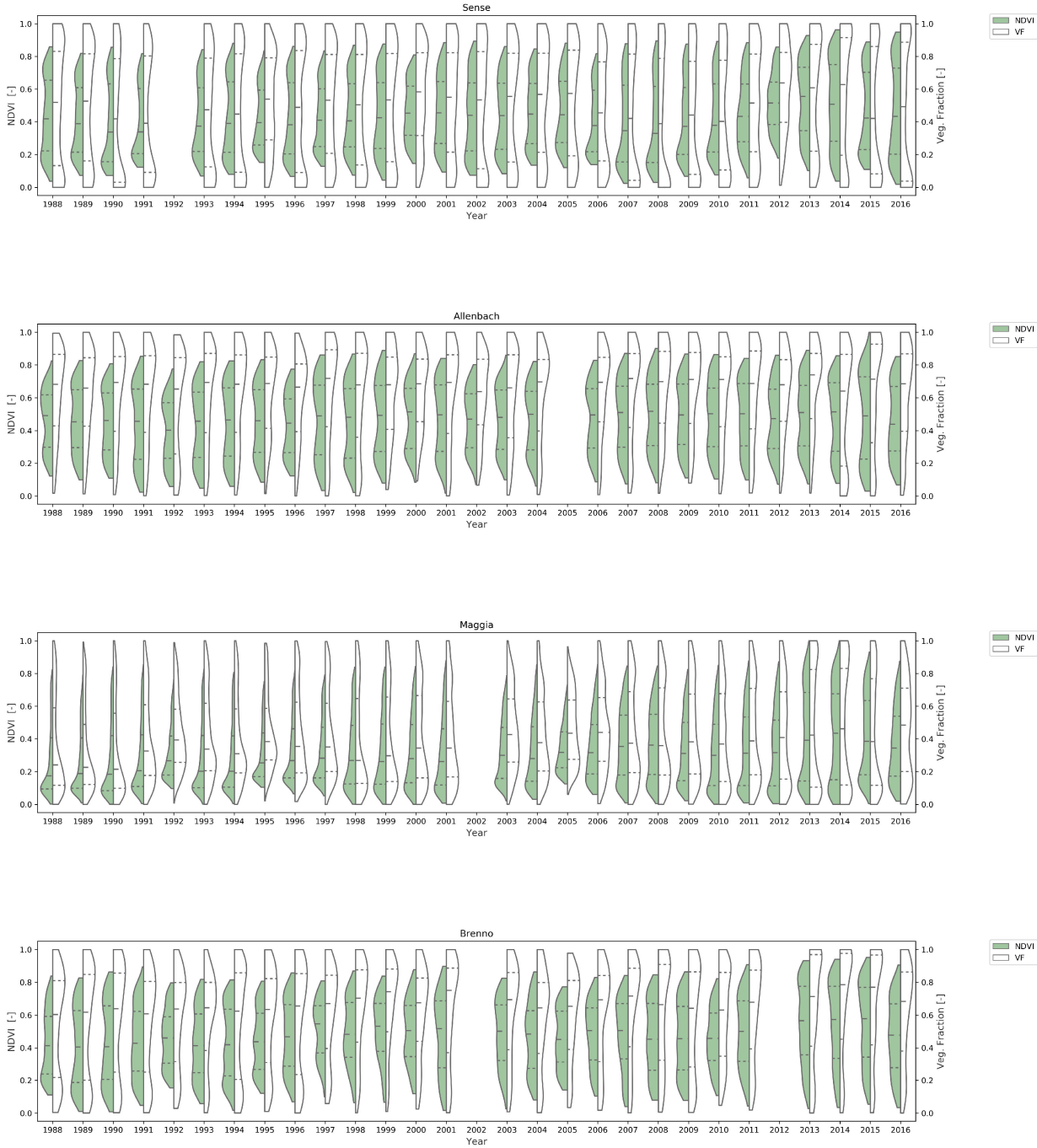

APPENDIX E
COMPLEMENTARY INFORMATION ON THE LINK BETWEEN VF AND OCCURRENCE OF *Q2* EVENTS

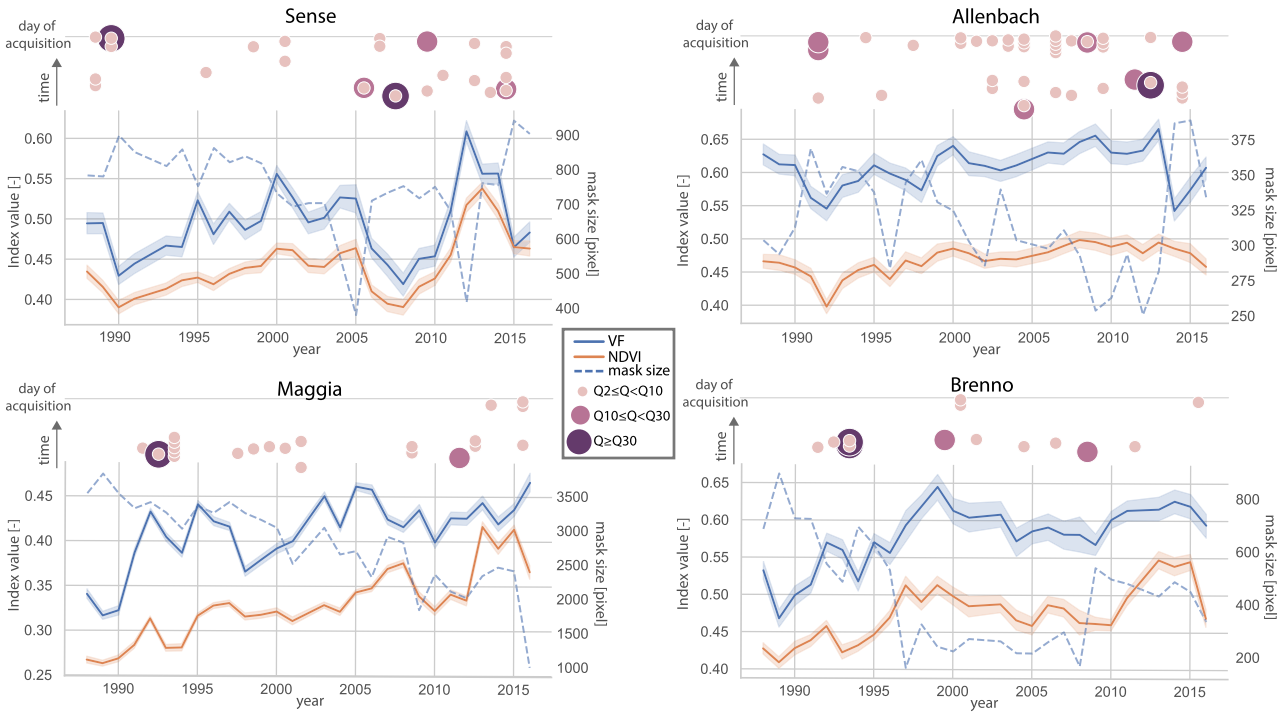

Fig. 9. Linear regression between the year of image acquisition and median of NDVI and VF. The colored areas represent a confidence interval of 68% for the regression line. Asterisk (*) indicates a p-value smaller than 0.05.

ACKNOWLEDGMENT

The authors would like to thank E. Casalini from the Remote Sensing Laboratories at UZH for providing background information.

REFERENCES

[1] K. Tockner and J. A. Stanford, "Riverine flood plains: Present state and future trends," *Environ. Conservation*, vol. 29, no. 3, pp. 308–330, 2002.
[2] S. R. Carpenter, E. H. Stanley, and M. J. V. Zanden, "State of the world's freshwater ecosystems: Physical, chemical, and biological changes," *Annu. Rev. Environ. Resour.*, vol. 36, pp. 75–99, 2011.
[3] C. Zarfl, A. E. Lumsdon, J. Berlekamp, L. Tydecks, and K. Tockner, "A global boom in hydropower dam construction," *Aquatic Sci.*, vol. 77, no. 1, pp. 161–170, 2015.
[4] S. Tealdi, C. Camporeale, and L. Ridolfi, "Modeling the impact of river damming on riparian vegetation," *J. Hydrology*, vol. 396, no. 3/4, pp. 302–312, 2011.
[5] G. Bornette and C. Amoros, "Disturbance regimes and vegetation dynamics: Role of floods in riverine wetlands," *J. Vegetation Sci.*, vol. 7, no. 5, pp. 615–622, 1996.
[6] C. R. Hupp and W. Osterkamp, "Riparian vegetation and fluvial geomorphic processes," *Geomorphology*, vol. 14, no. 4, pp. 277–295, 1996.
[7] N. L. Poff and J. K. Zimmerman, "Ecological responses to altered flow regimes: A literature review to inform the science and management of environmental flows," *Freshwater Biol.*, vol. 55, no. 1, pp. 194–205, 2010.
[8] F. C. Aguiar, M. J. Martins, P. C. Silva, and M. R. Fernandes, "Riverscapes downstream of hydropower dams: Effects of altered flows and historical land-use change," *Landscape Urban Planning*, vol. 153, pp. 83–98, 2016.
[9] A. Gurnell, "Plants as river system engineers," *Earth Surface Processes Landforms*, vol. 39, no. 1, pp. 4–25, 2014.
[10] A. Gurnell, W. Bertoldi, and D. Corenblit, "Changing river channels: The roles of hydrological processes, plants and pioneer fluvial landforms in humid temperate, mixed load, gravel bed rivers," *Earth-Sci. Rev.*, vol. 111, no. 1/2, pp. 129–141, 2012.
[11] C. Camporeale, E. Perucca, L. Ridolfi, and A. Gurnell, "Modeling the interactions between river morphodynamics and riparian vegetation," *Rev. Geophys.*, vol. 51, no. 3, pp. 379–414, 2013.
[12] A. Elosegi and S. Sabater, "Effects of hydromorphological impacts on river ecosystem functioning: A review and suggestions for assessing ecological impacts," *Hydrobiologia*, vol. 712, no. 1, pp. 129–143, 2013.
[13] J. Bendix and J. Stella, "Riparian vegetation and the fluvial environment: A biogeographic perspective," in *Treatise on Geomorphology*. New York, NY, USA: Elsevier, 2013, pp. 53–74.
[14] I. Van Splunder, H. Coops, L. Voesenek, and C. Blom, "Establishment of alluvial forest species in floodplains: The role of dispersal timing, germination characteristics and water level fluctuations," *Acta Botanica Neerlandica*, vol. 44, no. 3, pp. 269–278, 1995.
[15] I. Pattison, S. N. Lane, R. J. Hardy, and S. M. Reaney, "The role of tributary relative timing and sequencing in controlling large floods," *Water Resour. Res.*, vol. 50, no. 7, pp. 5444–5458, 2014.
[16] B. Belletti, S. Dufour, and H. Piégay, "Regional assessment of the multi-decadal changes in braided riverscapes following large floods (example of 12 reaches in South East of France)," *Advances Geosci.*, vol. 37, pp. 57–71, 2014.
[17] N. L. Poff *et al.*, "The natural flow regime," *BioScience*, vol. 47, no. 11, pp. 769–784, 1997.
[18] R. E. Tharme, "A global perspective on environmental flow assessment: Emerging trends in the development and application of environmental flow methodologies for rivers," *River Res. Appl.*, vol. 19, no. 5/6, pp. 397–441, 2003.

[19] W. Bertoldi, N. A. Drake, and A. Gurnell, "Interactions between river flows and colonizing vegetation on a braided river: Exploring spatial and temporal dynamics in riparian vegetation cover using satellite data," *Earth Surface Processes Landforms*, vol. 36, no. 11, pp. 1474–1486, 2011.

[20] J. Girel, "Large scale remote sensing and cartography of alluvial vegetation: Example of the low plain of the Ain river," *P. Ozenda, Documents de Cartographie Écologique*, vol. 29, pp. 45–74, 1986.

[21] M. Laba *et al.*, "Mapping invasive wetland plants in the hudson river national estuarine research reserve using quickbird satellite imagery," *Remote Sens. Environ.*, vol. 112, no. 1, pp. 286–300, 2008.

[22] R. J. Strick *et al.*, "Quantification of bedform dynamics and bedload sediment flux in sandy braided rivers from airborne and satellite imagery," *Earth Surface Processes Landforms*, vol. 44, no. 4, pp. 953–972, 2018.

[23] T. Strasser, S. Lang, B. Riedler, L. Pernkopf, and K. Paccagnel, "Multiscale object feature library for habitat quality monitoring in Riparian forests," *IEEE Geosci. Remote Sens. Lett.*, vol. 11, no. 2, pp. 559–563, Feb. 2014.

[24] P. Carbonneau and H. Piégay, *Fluvial Remote Sensing for Science and Management*. Hoboken, NJ, USA: Wiley, 2012.

[25] S. Bizzi, L. Demarchi, R. C. Grabowski, C. J. Weissteiner, and W. Van de Bund, "The use of remote sensing to characterise hydromorphological properties of european rivers," *Aquatic Sci.*, vol. 78, no. 1, pp. 57–70, 2016.

[26] Y. Chen, C. Huang, C. Ticehurst, L. Merrin, and P. Thew, "An evaluation of modis daily and 8-day composite products for floodplain and wetland inundation mapping," *Wetlands*, vol. 33, no. 5, pp. 823–835, 2013.

[27] L. Lymburner, A. McIntyre, F. Li, A. Ip, M. Thankappan, and J. Sixsmith, "Creating multi-sensor time series using data from landsat-5 TM and landsat-7 ETM+ to characterise vegetation dynamics," in *Proc. IEEE Int. Geosci. Remote Sens. Symp.*, 2013, pp. 961–963.

[28] F. Zhao, C. Huang, and Z. Zhu, "Use of vegetation change tracker and support vector machine to map disturbance types in greater yellowstone ecosystems in a 1984–2010 landsat time series," *IEEE Geosci. Remote Sens. Lett.*, vol. 12, no. 8, pp. 1650–1654, Aug. 2015.

[29] N. Kayastha, V. Thomas, J. Galbraith, and A. Banskota, "Monitoring wetland change using inter-annual landsat time-series data," *Wetlands*, vol. 32, no. 6, pp. 1149–1162, 2012.

[30] K. C. Fickas, W. B. Cohen, and Z. Yang, "Landsat-based monitoring of annual wetland change in the Willamette Valley of Oregon, USA from 1972 to 2012," *Wetlands Ecology Manage.*, vol. 24, no. 1, pp. 73–92, 2016.

[31] D. C. Whited, M. S. Lorang, M. J. Harner, F. R. Hauer, J. S. Kimball, and J. A. Stanford, "Climate, hydrologic disturbance, and succession: Drivers of floodplain pattern," *Ecology*, vol. 88, no. 4, pp. 940–953, 2007.

[32] J. Lejot, H. Piégay, P. D. Hunter, B. Moulin, and M. Gagnage, "Utilization of remote sensing for the characterization of river corridors: Examples of applications and current issues," *Géomorphologie: Relief, Processus, Environ.*, vol. 17, no. 2, pp. 157–172, 2011.

[33] G. P. Williams and M. G. Wolman, "Downstream effects of dams on Alluvial rivers," U.S. Geological Survey Professional Paper 1286, 1984.

[34] F. K. Ligon, W. E. Dietrich, and W. J. Trush, "Downstream ecological effects of dams," *BioScience*, vol. 45, no. 3, pp. 183–192, 1995.

[35] W. Gostner, M. Alp, A. J. Schleiss, and C. T. Robinson, "The hydromorphological index of diversity: A tool for describing habitat heterogeneity in river engineering projects," *Hydrobiologia*, vol. 712, no. 1, pp. 43–60, 2013.

[36] S. Rohde, F. Kienast, and M. Bürgi, "Assessing the restoration success of river widenings: A landscape approach," *Environ. Manage.*, vol. 34, no. 4, pp. 574–589, 2004.

[37] M. Döring *et al.*, "Artificial flood on the Saane River – eine measure on sustainable floodplain management," from German, *Wasser Energie Luft*, vol. 110, pp. 119–127, 2018.

[38] G. Milani *et al.*, "Robust quantification of riverine land cover dynamics by high-resolution remote sensing," *Remote Sens. Environ.*, vol. 217, pp. 491–505, 2018.

[39] G. Milani, M. Kneubühler, D. Tonolla, M. Doering, and M. E. Schaepman, "Remotely sensing variation in ecological strategies and plant traits of willows in perialpine floodplains," *J. Geophysical Res., Biogeosciences*, vol. 124, no. 7, pp. 2090–2106, 2019.

[40] R. G. Receanu, "Modélisation hydrologique des précipitations et des crues extrêmes dans les bassins versants alpin," Ph.D. dissertation, Faculté des géosciences et de l'environnement, Université de Lausanne, Lausanne, Switzerland, 2013.

[41] D. N. Collins, "Variability of runoff from Alpine Basins," *IAHS Publication*, vol. 308, pp. 466–472, 2006.

[42] P. Molnar, V. Favre, P. Perona, P. Burlando, C. Randin, and W. Ruf, "Floodplain forest dynamics in a hydrologically altered mountain river," *Peckiana*, vol. 5, pp. 17–24, 2008.

[43] P. Perona, P. Molnar, M. Savina, and P. Burlando, "An observation-based stochastic model for sediment and vegetation dynamics in the floodplain of an Alpine Braided river," *Water Resour. Res.*, vol. 45, no. 9, pp. 1–13, 2009.

[44] M. Brunke, "Floodplains of a regulated southern Alpine river (Bcrenno, Switzerland): Ecological assessment and conservation options," *Aquatic Conservation, Marine Freshwater Ecosystems*, vol. 12, no. 6, pp. 583–599, 2002.

[45] A. Tillack, A. Clasen, B. Kleinschmit, and M. Förster, "Estimation of the seasonal leaf area index in an alluvial forest using high-resolution satellite-based vegetation indices," *Remote Sens. Environ.*, vol. 141, pp. 52–63, 2014.

[46] "Landsat surface reflectance data," U.S. Geological Survey, Reston, VA, USA, Report 2015-3034, 2015.

[47] G. Chander, B. L. Markham, and D. L. Helder, "Summary of current radiometric calibration coefficients for landsat mss, tm, etm+, and eo-1 ali sensors," *Remote Sens. Environ.*, vol. 113, no. 5, pp. 893–903, 2009.

[48] B. L. Markham and D. L. Helder, "Forty-year calibrated record of earth-reflected radiance from landsat: A review," *Remote Sens. Environ.*, vol. 122, pp. 30–40, 2012.

[49] B. L. Markham, J. C. Storey, D. L. Williams, and J. R. Irons, "Landsat sensor performance: History and current status," *IEEE Trans. Geosci. Remote Sens.*, vol. 42, no. 12, pp. 2691–2694, Dec. 2004.

[50] J. Masek *et al.*, "Ledaps landsat calibration, reflectance, atmospheric correction preprocessing code," in *Proc. ORNL DAAC*, 2012, https://daac.ornl.gov/cgi-bin/dsviewer.pl?ds_id=1146.

[51] J. Ju, D. P. Roy, E. Vermote, J. Masek, and V. Kovalskyy, "Continental-scale validation of modis-based and ledaps landsat ETM+ atmospheric correction methods," *Remote Sens. Environ.*, vol. 122, pp. 175–184, 2012.

[52] J. R. Schott *et al.*, "The impact of improved signal-to-noise ratios on algorithm performance: Case studies for landsat class instruments," *Remote Sens. Environ.*, vol. 185, pp. 37–45, 2016.

[53] E. Vermote, C. Justice, M. Claverie, and B. Franch, "Preliminary analysis of the performance of the landsat 8/OLI land surface reflectance product," *Remote Sens. Environ.*, vol. 185, pp. 46–56, 2016.

[54] J. W. Rouse Jr, R. H. Haas, J. Schell, and D. Deering, "Monitoring the vernal advancement and retrogradation (green wave effect) of natural vegetation," Remote Sensing Center, Texas A&M Univ., College Station, TX, USA, Tech. Rep. E73-10693, NASA-CR-132982, 1973.

[55] J. W. Boardman, "Geometric mixture analysis of imaging spectrometry data," in *Proc. IEEE Int. Geosci. Remote Sens. Symp.*, 1994, vol. 4, pp. 2369–2371.

[56] D. P. Turner, W. B. Cohen, R. E. Kennedy, K. S. Fassnacht, and J. M. Briggs, "Relationships between leaf area index and landsat TM spectral vegetation indices across three temperate zone sites," *Remote Sens. Environ.*, vol. 70, no. 1, pp. 52–68, 1999.

[57] T. Bellone, P. Boccardo, and F. Perez, "Investigation of vegetation dynamics using long-term normalized difference vegetation index time-series," *Amer. J. Environ. Sci.*, vol. 5, no. 4, pp. 460–466, 2009.

[58] N. Pettorelli, J. O. Vik, A. Mysterud, J.-M. Gaillard, C. J. Tucker, and N. C. Stenseth, "Using the satellite-derived NDVI to assess ecological responses to environmental change," *Trends Ecology Evolution*, vol. 20, no. 9, pp. 503–510, 2005.

[59] A. J. Peters, E. A. Walter-Shea, L. Ji, A. Vina, M. Hayes, and M. D. Svoboda, "Drought monitoring with NDVI-based standardized vegetation index," *Photogrammetric Eng. Remote Sens.*, vol. 68, no. 1, pp. 71–75, 2002.

[60] M. Forkel, N. Carvalhais, J. Verbesselt, M. D. Mahecha, C. S. Neigh, and M. Reichstein, "Trend change detection in NDVI time series: Effects of inter-annual variability and methodology," *Remote Sens.*, vol. 5, no. 5, pp. 2113–2144, 2013.

[61] N. Keshava and J. F. Mustard, "Spectral unmixing," *IEEE Signal Process. Mag.*, vol. 19, no. 1, pp. 44–57, Jan. 2002.

[62] Z. Mitraka, F. Del Frate, and F. Carbone, "Nonlinear spectral unmixing of landsat imagery for urban surface cover mapping," *IEEE J. Sel. Topics Appl. Earth Observ. Remote Sens.*, vol. 9, no. 7, pp. 3340–3350, Jul. 2016.

[63] A. Baldridge, S. Hook, C. Grove, and G. Rivera, "The aster spectral library version 2.0," *Remote Sens. Environ.*, vol. 113, no. 4, pp. 711–715, 2009.

[64] L. W. Mays, *Water Resources Engineering*. Hoboken, NJ, USA: Wiley, 2010.

[65] A. Te Linde, J. Aerts, A. Bakker, and J. Kwadijk, "Simulating low-probability peak discharges for the Rhine basin using resampled climate modeling data," *Water Resour. Res.*, vol. 46, no. 3, pp. 1–19, 2010.

[66] G. Villarini, J. A. Smith, F. Serinaldi, and A. A. Ntelekos, "Analyses of seasonal and annual maximum daily discharge records for central Europe," *J. Hydrology*, vol. 399, no. 3/4, pp. 299–312, 2011.

[67] D. Meissner, B. Klein, and M. Ionita, "Development of a monthly to seasonal forecast framework tailored to inland waterway transport in Central Europe," *Hydrology Earth Syst. Sci.*, vol. 21, pp. 6401–6423, 2017.

[68] K. Tockner, M. S. Lorang, and J. A. Stanford, "River flood plains are model ecosystems to test general hydrogeomorphic and ecological concepts," *River Res. Appl.*, vol. 26, no. 1, pp. 76–86, 2010.

[69] L. Harrison, C. Legleiter, M. Wydzga, and T. Dunne, "Channel dynamics and habitat development in a meandering, gravel bed river," *Water Resour. Res.*, vol. 47, no. 4, pp. 1–21, 2011.

[70] F. J. Magilligan, E. Buraas, and C. Renshaw, "The efficacy of stream power and flow duration on geomorphic responses to catastrophic flooding," *Geomorphology*, vol. 228, pp. 175–188, 2015.

[71] S. Lallias-Tacon, F. Liébault, and H. Piégay, "Use of airborne lidar and historical aerial photos for characterising the history of braided river floodplain morphology and vegetation responses," *Catena*, vol. 149, pp. 742–759, 2017.

[72] C. Ilg *et al.*, "Long-term reactions of plants and macroinvertebrates to extreme floods in floodplain grasslands," *Ecology*, vol. 89, no. 9, pp. 2392–2398, 2008.

[73] V. Garófano-Gómez, F. Martínez-Capel, W. Bertoldi, A. Gurnell, J. Estornell, and F. Segura-Beltrán, "Six decades of changes in the riparian corridor of a Mediterranean river: A synthetic analysis based on historical data sources," *Ecohydrology*, vol. 6, no. 4, pp. 536–553, 2013.

[74] D. B. Arscott, K. Tockner, D. van der Nat, and J. Ward, "Aquatic habitat dynamics along a braided alpine river ecosystem (Tagliamento River, Northeast Italy)," *Ecosystems*, vol. 5, no. 8, pp. 0802–0814, 2002.

[75] D. Knighton, *Fluvial Forms and Processes: A New Perspective*. Evanston, IL, USA: Routledge, 2014.

[76] E. Wohl *et al.*, "The natural sediment regime in rivers: Broadening the foundation for ecosystem management," *BioScience*, vol. 65, no. 4, pp. 358–371, 2015.

[77] C. A. Bateson, G. P. Asner, and C. A. Wessman, "Endmember bundles: A new approach to incorporating endmember variability into spectral mixture analysis," *IEEE Trans. Geosci. Remote Sens.*, vol. 38, no. 2, pp. 1083–1094, Mar. 2000.

[78] R. Receanu, J.-A. Hertig, J.-M. Fallot, and T. E. Man, "Determination of extreme floods using a distributed hydrological model," *Bull. Polytehnica Univ. Timisoara (Romania), Trans. Hydrotechnics*, vol. 56, no. 1, pp. 33–36, 2011.

[79] J. C. Stromberg and D. T. Patten, "Early recovery of an eastern sierra nevada riparian system after 40 years of stream diversion," in *Proc. California Riparian Syst. Conf., Protection, Manage. Restoration1990s*, 1989, vol. 110, pp. 399–404.

[80] D. H. Kim, H. Choi, and J. G. Kim, "Occupational strategy of persicaria thunbergii in riparian area: Rapid recovery after harsh flooding disturbance," *J. Plant Biol.*, vol. 55, no. 3, pp. 226–232, 2012.

[81] N. C. Sims and M. J. Colloff, "Remote sensing of vegetation responses to flooding of a semi-arid floodplain: Implications for monitoring ecological effects of environmental flows," *Ecological Indicators*, vol. 18, pp. 387–391, 2012.

[82] K. Tockner, F. Malard, and J. Ward, "An extension of the flood pulse concept," *Hydrological Processes*, vol. 14, no. 16/17, pp. 2861–2883, 2000.

[83] J. Steiger and A. M. Gurnell, "Spatial hydrogeomorphological influences on sediment and nutrient deposition in riparian zones: Observations from the garonne river, france," *Geomorphology*, vol. 49, no. 1/2, pp. 1–23, 2003.

[84] D. Walling, Q. He, and W. Blake, "River flood plains as phosphorus sinks," *IAHS Publication (Int. Assoc. Hydrological Sci.)*, no. 263, pp. 211–218, 2000.

[85] E. González, E. Muller, F. A. Comín, and M. González-Sanchis, "Leaf nutrient concentration as an indicator of populus and tamarix response to flooding," *Perspectives Plant Ecology, Evol. Systematics*, vol. 12, no. 4, pp. 257–266, 2010.

[86] D. Hering, M. Gerhard, R. Manderbach, and M. Reich, "Impact of a 100-year flood on vegetation, benthic invertebrates, riparian fauna and large woody debris standing stock in an alpine floodplain," *River Res. Appl.*, vol. 20, no. 4, pp. 445–457, 2004.

[87] S. J. Capon *et al.*, "Riparian ecosystems in the 21st century: Hotspots for climate change adaptation?" *Ecosystems*, vol. 16, no. 3, pp. 359–381, 2013.

[88] P. W. Bogaart and R. T. Van Balen, "Numerical modeling of the response of alluvial rivers to quaternary climate change," *Global Planetary Change*, vol. 27, no. 1–4, pp. 147–163, 2000.

[89] J. C. Knox, "Sensitivity of modern and holocene floods to climate change," *Quaternary Sci. Rev.*, vol. 19, no. 1–5, pp. 439–457, 2000.

[90] L. Ström, R. Jansson, and C. Nilsson, "Projected changes in plant species richness and extent of riparian vegetation belts as a result of climate-driven hydrological change along the vindel river in Sweden," *Freshwater Biol.*, vol. 57, no. 1, pp. 49–60, 2012.

[91] R. Rivaes, P. M. Rodríguez-González, A. Albuquerque, A. N. Pinheiro, G. Egger, and M. T. Ferreira, "Riparian vegetation responses to altered flow regimes driven by climate change in mediterranean rivers," *Ecohydrology*, vol. 6, no. 3, pp. 413–424, 2013.

[92] D. Sulla-Menashe, M. A. Friedl, and C. E. Woodcock, "Sources of bias and variability in long-term landsat time series over Canadian boreal forests," *Remote Sens. Environ.*, vol. 177, pp. 206–219, 2016.

[93] C. E. Holden and C. E. Woodcock, "An analysis of landsat 7 and landsat 8 underflight data and the implications for time series investigations," *Remote Sens. Environ.*, vol. 185, pp. 16–36, 2016.

[94] D. Helder *et al.*, "Observations and recommendations for the calibration of landsat 8 OLI and sentinel 2 MSI for improved data interoperability," *Remote Sens.*, vol. 10, no. 9, pp. 1340–1369, 2018.

[95] B. Somers, G. P. Asner, L. Tits, and P. Coppin, "Endmember variability in spectral mixture analysis: A review," *Remote Sens. Environ.*, vol. 115, no. 7, pp. 1603–1616, 2011.

[96] A. J. Elmore, J. F. Mustard, S. J. Manning, and D. B. Lobell, "Quantifying vegetation change in semiarid environments: Precision and accuracy of spectral mixture analysis and the normalized difference vegetation index," *Remote Sens. Environ.*, vol. 73, no. 1, pp. 87–102, 2000.

[97] R. Sonnenschein, T. Kuemmerle, T. Udelhoven, M. Stellmes, and P. Hostert, "Differences in landsat-based trend analyses in drylands due to the choice of vegetation estimate," *Remote Sens. Environ.*, vol. 115, no. 6, pp. 1408–1420, 2011.

[98] J. Bendix and J. Stella, "Riparian vegetation and the fluvial environment: A biogeographic perspective," in *Treatise on Geomorphology*, J. F. Shroder, Ed. San Diego, CA, USA: Academic, 2013, pp. 53–74.

[99] F. Caponi, A. Koch, W. Bertoldi, D. F. Vetsch, and A. Siviglia, "When does vegetation establish on gravel bars? observations and modelling in the Alpine Rhine river," *Frontiers Environ. Sci.*, vol. 7, pp. 124–142, 2019.

[100] P. Humphries and D. S. Baldwin, "Drought and aquatic ecosystems: An introduction," *Freshwater Biol.*, vol. 48, no. 7, pp. 1141–1146, 2003.

[101] N. M. Amlin and S. B. Rood, "Drought stress and recovery of riparian cottonwoods due to water table alteration along Willow Creek, Alberta," *Trees*, Springer, vol. 17, no. 4, pp. 351–358, 2003.

[102] S. B. Rood, J. H. Braatne, and F. M. Hughes, "Ecophysiology of riparian cottonwoods: Stream flow dependency, water relations and restoration," *Tree Physiology*, vol. 23, no. 16, pp. 1113–1124, 2003.

[103] A. Karnieli *et al.*, "Use of NDVI and land surface temperature for drought assessment: Merits and limitations," *J. Climate*, vol. 23, no. 3, pp. 618–633, 2010.

[104] L. L. Hess, J. M. Melack, S. Filoso, and Y. Wang, "Delineation of inundated area and vegetation along the Amazon floodplain with the SIR-C synthetic aperture radar," *IEEE Trans. Geosci. Remote Sens.*, vol. 33, no. 4, pp. 896–904, Jul. 1995.

[105] J.-M. Martinez and T. Le Toan, "Mapping of flood dynamics and spatial distribution of vegetation in the amazon floodplain using multitemporal sar data," *Remote Sens. Environ.*, vol. 108, no. 3, pp. 209–223, 2007.

[106] E. J. Rignot, R. Zimmermann, and J. J. van Zyl, "Spaceborne applications of p band imaging radars for measuring forest biomass," *IEEE Trans. Geosci. Remote Sens.*, vol. 33, no. 5, pp. 1162–1169, Sep. 1995.

[107] C. da Costa Freitas *et al.*, "Land use and land cover mapping in the Brazilian Amazon using polarimetric airborne P-band SAR data," *IEEE Trans. Geosci. Remote Sens.*, vol. 46, no. 10, pp. 2956–2970, Oct. 2008.

[108] G. D. De Grandi, R. M. Lucas, and J. Kropacek, "Analysis by wavelet frames of spatial statistics in sar data for characterizing structural properties of forests," *IEEE Trans. Geosci. Remote Sens.*, vol. 47, no. 2, pp. 494–507, Feb. 2009.

[109] K. Tockner, M. Push, D. Borchardt, and M. S. Lorang, "Multiple stressors in coupled riverfloodplain ecosystems," *Freshwater Biol.*, vol. 55, no. s1, pp. 135–151, 2010.

[110] M. Waskom *et al.*, "mwaskom/seaborn: v0.8.1 (september 2017)," *Zenodo*, vol. 883859, Sep. 2017, https://doi.org/10.5281/zenodo.